Title

FAP20 is an inner junction protein of doublet microtubules essential for both the planar asymmetrical waveform and stability of flagella in Chlamydomonas.

Permalink

Journal

Authors

Yanagisawa, Haru-aki
Mathis, Garrison
Oda, Toshiyuki
et al.

Publication Date

DOI

FAP20 is an inner junction protein of doublet microtubules essential for both the planar asymmetrical waveform and stability of flagella in *Chlamydomonas*

Haru-aki Yanagisawa[a], Garrison Mathis[b], Toshiyuki Oda[a], Masafumi Hirono[c], Elizabeth A. Richey[b], Hiroaki Ishikawa[d], Wallace F. Marshall[d], Masahide Kikkawa[a], and Hongmin Qin[b]

[a]Department of Cell Biology and Anatomy, Graduate School of Medicine, and [c]Department of Biological Sciences, Graduate School of Science, University of Tokyo, 7-3-1 Hongo, Bunkyo-ku, Tokyo 113-0033, Japan; [b]Department of Biology, Texas A&M University, College Station, TX 77843; [d]Department of Biochemistry and Biophysics, University of California, San Francisco, San Francisco, CA 94158

ABSTRACT The axoneme—the conserved core of eukaryotic cilia and flagella—contains highly specialized doublet microtubules (DMTs). A long-standing question is what protein(s) compose the junctions between two tubules in DMT. Here we identify a highly conserved flagellar-associated protein (FAP), FAP20, as an inner junction (IJ) component. The flagella of *Chlamydomonas* FAP20 mutants have normal length but beat with an abnormal symmetrical three-dimensional pattern. In addition, the mutant axonemes are liable to disintegrate during beating, implying that interdoublet connections may be weakened. Conventional electron microscopy shows that the mutant axonemes lack the IJ, and cryo–electron tomography combined with a structural labeling method reveals that the labeled FAP20 localizes at the IJ. The mutant axonemes also lack doublet-specific beak structures, which are localized in the proximal portion of the axoneme and may be involved in planar asymmetric flagellar bending. FAP20 itself, however, may not be a beak component, because uniform localization of FAP20 along the entire length of all nine DMTs is inconsistent with the beak's localization. FAP20 is the first confirmed component of the IJ. Our data also suggest that the IJ is important for both stabilizing the axoneme and scaffolding intra–B-tubular substructures required for a planar asymmetrical waveform.

INTRODUCTION

Cilia and flagella are conserved organelles projecting from the surface of nearly all eukaryotic cells and have been adapted for multiple uses, such as bulk fluid movement, cellular motility, and sensing of extracellular signals (Ishikawa and Marshall, 2011). These organelles are important for human health since ciliary defects have been implicated in a broad spectrum of human diseases, such as primary ciliary dyskinesia, nephronophthisis, retinal degeneration, situs inversus, hydrocephalus, polydactyly, and obesity (Hildebrandt *et al.*, 2011).

Highly specialized doublet microtubules (DMTs), templated by the basal bodies, are cylindrically arranged to form the essential and conserved framework of cilia and flagella. Many structures, including outer and inner arm dyneins, radial spokes, and the dynein regulatory complex (DRC), are assembled onto DMTs in a highly specific manner to produce the integrated axoneme (Dutcher, 1995). A unique, asymmetrical morphology of DMTs should be important for both the site-specific attachment of these structures and mechanical properties of the axoneme. The A-tubules of DMTs are composed of 13 tubulin protofilaments (PFs), similar to cytoplasmic microtubules (MTs), whereas the B-tubules are incomplete, C-shaped tubules

composed of 10 PFs and one smaller subunit (Nicastro et al., 2011). A long-standing question concerns how the junctions between the two tubules in the DMT are formed (Linck and Stephens, 2007). The two junctions between the A- and B-tubules are structurally different: the outer junction is formed by close, unusual interactions among three tubulin PFs, whereas the inner junction (IJ) is formed by the smaller subunit, composed of nontubulin protein(s) that bridge tubulin PFs of the A- and B-tubules (Nicastro et al., 2011). Formation of B-tubule–like "hooks" onto preexisting axonemal and mitotic spindle MTs can be induced by adding purified brain tubulins (Euteneuer and McIntosh, 1980). The hooks initiate by forming outer-like junctions but barely close by forming inner-like junctions, supporting the notion that nontubulin protein is indispensable for the IJ.

Biochemical and proteomic studies of the axonemes have identified potential candidates for the nontubulin protein(s) in the DMT. The PF ribbon, which is resistant to Sarkosyl extraction, contains tektins (Linck et al., 1982; Yanagisawa and Kamiya, 2004), Rib72/EFhc1 (Ikeda et al., 2003), and Rib43a (Norrander et al., 2000). Parkin coregulated gene product (PACRG) was identified as an interacting protein of Rib72 (Ikeda et al., 2007). Because the PF ribbon is believed to derive from the A-tubule PFs near the IJ (Witman et al., 1972; Linck et al., 1982), it is possible that these proteins are involved in formation of the IJ. However, localization and functions of these proteins in the DMT are unclear due to lack of detailed structural analysis. In addition to these known proteins, we previously found several unidentified proteins tightly associated with the A-tubule after detergent extractions (Yanagisawa and Kamiya, 2004), which solubilize the B-tubule, leaving junctional PFs (Witman et al., 1972). The Chlamydomonas flagella proteome contained a large number of uncharacterized proteins in the salt-extracted axoneme fraction, which contained DMTs. Therefore these proteins were potential candidates for the junctional proteins of the DMT.

In this study, we focus on a highly conserved flagellar-associated protein (FAP), FAP20, found in the Chlamydomonas flagellar proteome and analyze its function using Chlamydomonas mutants that completely lack FAP20. The mutants have motility defects with an abnormal, symmetrical waveform and lack doublet-specific structures. In addition, the axonemes of the mutants exhibit reduced stability in the connection between DMTs. To explain these functional phenotypes, we structurally determined that FAP20 is a component of the IJ using both conventional electron microscopy and cryo–electron tomography. We discuss the function of the IJ in relation to the phenotypes of FAP20 mutants.

RESULTS

FAP20 is a candidate for a junctional component of DMT

To identify novel candidate proteins for the junctional proteins of the DMT, we used the Chlamydomonas flagellar proteome database, in which biochemically fractionated flagella were analyzed (Pazour et al., 2005). The candidates were selected according to three criteria: they are 1) mainly contained in the KCl-insoluble fraction; 2) as abundant as components of other known axonemal structures, for example, dyneins or radial spokes, but are not components of these structures; and 3) highly conserved among organisms with cilia and flagella. One of the candidates, FAP20, is predominantly detected in the KCl-insoluble fraction, and the number of detected peptides is comparable to those of radial spoke or dynein components. In addition, FAP20 has two prominent features: it is very basic, with a PI of 9.6, and is extremely conserved across species; Chlamydomonas and human homologues share 89% identical and 94% similar amino acid sequences. FAP20 is also found in the Chlamydomonas basal

body proteome (Keller et al., 2005) and annotated as BUG22p (basal-body proteins with upregulated genes 22). Studies in other organisms show that FAP20 homologues localize to the cilia or flagella (Laligne et al., 2010; Hodges et al., 2011; Ishikawa et al., 2012), and FAP20-depleted paramecia have motility defects with an altered waveform (Laligne et al., 2010). Therefore we focus on FAP20 here.

FAP20 is mutated in motility mutants, *dmj1*

We assumed that the FAP20 mutant cells can produce flagella but cannot swim forward because of altered rigidity of their flagella. We therefore first isolated the mutants that sink to the bottom of liquid cultures and then used a low-magnification microscope to identify the ones just trembling or rotating instead of swimming fast like wild-type cells. Four alleles of FAP20 mutants were isolated from different libraries of motility mutants. These mutants were named *doublet microtubule junction 1* or *dmj1* because FAP20 is a component of the inner junction of DMTs (data shown later). The first allele, *dmj1-1*, was created by insertional mutagenesis, but the plasmid insertion was not linked to the motility phenotype. Thus we mapped the mutation by amplified fragment length polymorphism (AFLP) analysis and sequencing of FAP genes (Pazour et al., 2005) contained in the mapped region. We found the *dmj1-1* has a mutation in the gene encoding FAP20 (Figure 1A and Supplemental Figure S1, A and B). In addition to *dmj1-1*, two alleles, *dmj1-2* and *dmj1-3*, were identified from similarity of the motility phenotype (Figure 1A
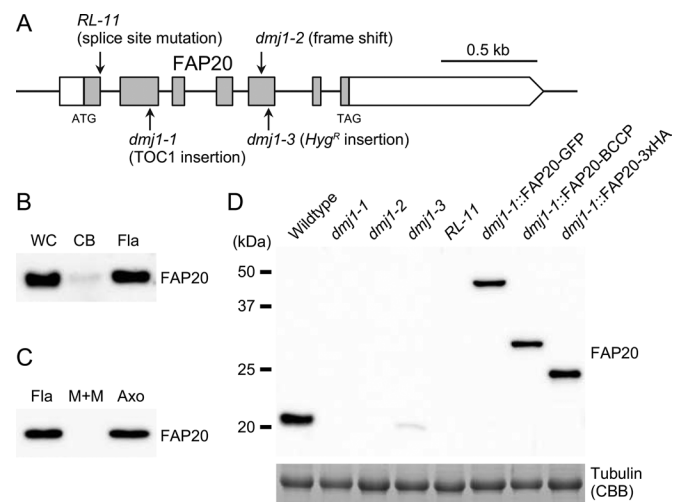
FIGURE 1: Four mutant alleles of *dmj1*. (A) The mutation sites of four different *dmj1* alleles are indicated on the exon/intron structure of the FAP20 gene (Cre07.g351650.t1.3 in Phytozome v9.1; www.phytozome.net/). The details of the mutations are described in Supplemental Figure S1. (B) FAP20 protein is mainly present in flagella. Whole-cell (WC), cell body without flagella (CB), and flagella (Fla) samples were analyzed by Western blotting with anti-FAP20 antibody. The WC and CB lanes contain the same number of cells. *Chlamydomonas* cells have two flagella; thus twice as many flagella as cell bodies were loaded in the Fla lane. (C) FAP20 protein is associated with the axoneme. Flagella (Fla), membrane and matrix (M+M), and axonemal (Axo) samples were analyzed by Western blotting with anti-FAP20 antibody. (D) Western blot analysis of axonemes from the FAP20 mutants and rescued strains with FAP20 antibody. The axonemes of *dmj1-1*, *dmj1-2*, and *RL-11* completely lack the FAP20 protein. The axoneme of *dmj1-3* contains reduced amount of a truncated FAP20 protein. The axonemes of the rescued strains contain wild-type amounts of the GFP-, BCCP-, and 3xHA-tagged FAP20 proteins. Coomassie-stained bands of tubulins were used as a loading control.

and Supplemental Figure S1A). We also found that the strain *RL-11* (Reverse Locomotion 11; Nakamura, 1981), which was reported as a backward-swimming mutant, is allelic to the *dmj1* mutation (Figure 1A and Supplemental Figure S1A).

To characterize the localization and functions of the FAP20 in *Chlamydomonas*, we raised two rabbit polyclonal antibodies using the full-length recombinant FAP20 protein as antigens. Antibody #1 recognized a single 21-kDa band corresponding to FAP20 both in the whole-cell and axonemal samples, whereas antibody #2 recognized an additional 37-kDa nonspecific band only in the whole-cell sample (Supplemental Figure S2A). We thus mainly use antibody #1 in the following analyses. Because the hygromycin B resistance gene is inserted to the near 3′ end of the FAP20-coding sequence, the strain *dmj1-3* is expected to produce a truncated FAP20 protein lacking the C-terminal 20 amino acids (Supplemental Figure S1, A and C). Western blot analysis showed that only antibody #2 recognizes full-length and truncated proteins equally well, whereas antibody #1 preferably recognizes the full-length protein (Supplemental Figure S2B). To exclude the possibility that the weak signal for *dmj1-3* on Western blots is due to the failure of antibody reacting to the C-terminal–truncated mutant protein, we used antibody #2 for analyses including the *dmj1-3* strain.

We first biochemically examined the localization of FAP20. Western blot analysis clearly showed that most of FAP20 is present in the flagella, with a trace amount in cell bodies (Figure 1B). Another Western blot analysis of fractionated flagella showed that the FAP20 is associated with the axoneme (Figure 1C), consistent with the result of the *Chlamydomonas* flagellar proteome (Pazour et al., 2005). The axonemes of the three alleles, *dmj1-1*, *dmj1-2*, and *RL-11*, completely lacked the FAP20 protein, whereas *dmj1-3* contained a reduced amount of the truncated FAP20 (Figure 1D and Supplemental Figure S2C).

We transformed *dmj1-1* cells with FAP20 genes tagged with green fluorescent protein (GFP), biotin carboxyl carrier protein (BCCP), and triple hemagglutinin (3xHA) to produce the three rescued strains *dmj1-1*::FAP20-GFP, *dmj1-1*::FAP20-BCCP, and *dmj1-1*::FAP20-3xHA, respectively. The transgene products were incorporated into the axonemes at comparable amounts to that of wild type (Figure 1D). In the following analyses, we label *dmj1-1* as *fap20null*, *dmj1-3* as *fap20ΔC*, *dmj1-1*::FAP20-GFP as *FAP20-GFP*, *dmj1-1*::FAP20-BCCP as *FAP20-BCCP*, and *dmj1-1*::FAP20-3xHA as *FAP20-3xHA* (Table 1).

FAP20 is not essential for flagellar assembly

Although FAP20 has been reported to be associated with both the flagella and the basal bodies, the FAP20 mutants did not exhibit any basal-body-related phenotypes, such as abnormality in number and positioning of flagella (unpublished data). The FAP20 mutants produced nearly wild-type length of flagella on average (Figure 2A). The *RL-11* strain produced slightly longer flagella than wild type, which is consistent with the original report (Nakamura, 1981). The FAP20 mutants also regenerated their flagella normally (unpublished data). Flagella of the FAP20 mutant alleles had a wider distribution of lengths ($p < 0.005$ for *fap20null* and *RL-11*, $p < 0.05$ for *fap20ΔC* by F test of equality of variances) than did those of wild type. These results suggest that FAP20 is not essential for flagellar assembly in *Chlamydomonas*.

FAP20 is essential for establishing the asymmetrical waveform and beating plane

Motility phenotypes of the *RL-11* mutant were previously reported (Nakamura, 1981), and we confirmed those phenotypes in the new FAP20 mutants. In contrast to wild-type cells, which swam in relatively continuous straight paths (Supplemental Video S1), *fap20null* cells appeared to twitch violently as they tumbled uncontrollably in every direction (Supplemental Video S2). Unlike the previous report, both the *RL-11* and our null alleles barely swam backward. The *fap20ΔC* cells, which express a C-terminal–truncated FAP20 protein, exhibited a mixed phenotype ranging from nearly wild type to the null mutant (Supplemental Video S3). The motility defects were rescued in *FAP20-GFP* and *FAP20-BCCP* strains, which expressed tagged wild-type FAP20 genes (Figures 2B and 1D and Supplemental Videos S4 and S6), confirming the absence of FAP20 as the cause of the motility defects.

Wild-type cells normally swim forward using an asymmetrical waveform, whereas the cells swim backward using a symmetrical waveform when stimulated by intense light (Figure 2C and Supplemental Video S6). As observed in the previous report for *RL-11* (Nakamura, 1981), the flagella of the *fap20null* strain beat with an abnormal, symmetrical waveform. We therefore also included the *mbo2* mutant, which displays only a symmetrical waveform (Segal et al., 1984), in this study for comparison (Supplemental Videos S5 and S6). The waveform of the *fap20null* strain has an abnormally large amplitude and increased bending at the proximal region compared with the symmetrical waveforms of wild type or *mbo2* (Figure 2C and Supplemental Video S6). In addition, the two flagella of the *fap20null* cell were often uncoordinated with each other (Figure 2C and Supplemental Video S6). These abnormalities prevented the *fap20null* cells from swimming backward, and instead they vibrated or rotated in circles. The *fap20ΔC* mutant cultures contained cells with mixed phenotypes. Some of them displayed an intermediate phenotype with flagella beat asymmetrically at the proximal region

Strain	Abbreviation	Phenotype	FAP20 mutation
dmj1-1	*fap20null*	Trembling	Null (TOC1 insertion)
dmj1-2	–	Trembling	Null (UV, frame shift)
dmj1-3	*fap20ΔC*	Mixed	ΔC 20 amino acids (*Hyg^R* insertion), reduced protein level
RL-11	–	Trembling	Null (UV, splice site mutation)
dmj1-1::FAP20-GFP	*FAP20-GFP*	Wild type	Rescued
dmj1-1::FAP20-BCCP	*FAP20-BCCP*	Wild type	Rescued
dmj1-1::FAP20-3xHA	*FAP20*-3xHA	Wild type	Rescued
sup-pf1-1 dmj1-1::FAP20-GFP	*sup-pf1 FAP20-GFP*	Slow swimming	Rescued

TABLE 1: *dmj1* alleles and rescued strains.
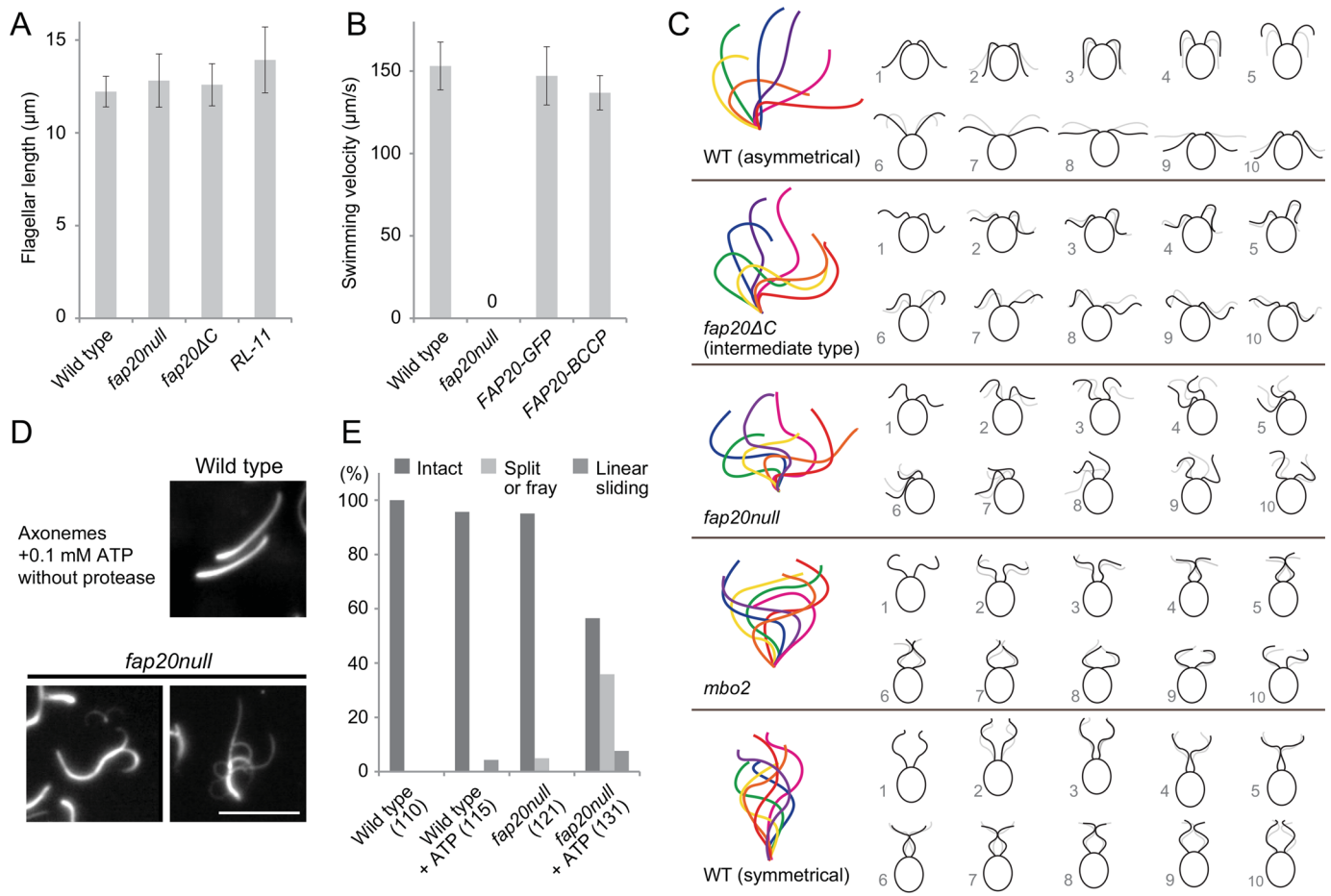
FIGURE 2: FAP20 is essential for both asymmetrical waveform and stability of flagella. (A) FAP20 mutants produce wild-type length of the flagella ($n = 33$). (B) Introduction of the tagged FAP20 constructs rescued the motility defect of the FAP20 mutant ($n = 30$). Error bars represent SD. (C) Waveforms from representative cells of wild type and each mutant allele as traced from recorded videos. Time between frames 1 and 10 is 0.02, 0.02, 0.033, 0.02, and 0.01 s, respectively, for WT (asymmetrical), *fap20ΔC* (intermediate type), *fap20null*, *mbo2*, and WT (symmetrical). (D) The axoneme of *fap20null* strain was unstable and liable to split or fray during beating. Demembranated axonemes of wild type and *fap20null* were reactivated with 0.1 mM ATP in presence of protease inhibitors. Bar, 10 μm. (E) Quantitative analysis of the disintegration of axonemes. Values in parentheses represent number of axonemes used for analyses.

but symmetrically at the distal region (Figure 2C and Supplemental Video S6). The reduction in severity of the beating defects in some *fap20ΔC* cells is likely due to the small amount of FAP20 in their flagella.

During the waveform analyses, we noticed that flagella of the *fap20null* cell often went out of the focal plane during beating cycles (Supplemental Video S6), suggesting a three-dimensional bending of the flagella. This barely occurred in wild-type and *mbo2* flagella. This loss of planar control is a major difference between the motility of *fap20null* and *mbo2* mutants.

FAP20 is essential for stability of the axoneme
We examined the stability of the axoneme of the *fap20null* strain, since the axoneme of the *RL-11* strain was reported to be disintegrated when reactivated with ATP (Nakamura, 1981). To prevent proteolysis of axonemal proteins, were demembranated axonemes and reactivated them in buffer containing protease inhibitors. On addition of ATP, both wild-type and *fap20null* axonemes started to beat vigorously. Unlike wild type, axonemes of *fap20null* cells often split or frayed during beating (Figure 2, D and E), suggesting that

connections between DMTs are weakened. The base of the axonemes tended to remain connected after disintegration (Figure 2D), consistent with a previous report (Bower *et al.*, 2013).

The axoneme of the FAP20 mutant lacks beak structures
To examine the structural defects that cause aberrant flagellar beating of the *fap20null* strain, we analyzed the ultrastructure of the axoneme using thin-section electron microscopy. The *fap20null* axonemes had normal arrangements of nine outer DMTs, two central singlet MTs, inner/outer dynein arms, and radial spokes. Moreover, the unique bridge present only between DMT1 and 2 and the loss of the outer arm dynein on DMT1 (Hoops and Witman, 1983) were also observed in the *fap20null* axonemes (Figure 3). One of the defects detected in the *fap20null* was in an intratubular structure called the "beak." In wild type, each of the proximal B-tubule lumens of DMT1, 5, and 6 contains a beak structure, which is believed to be related to the direction of flagellar bending (Hoops and Witman, 1983; Segal *et al.*, 1984; Figure 3). We found that the *fap20null* axoneme lacks these beak structures in all three DMTs (Figure 3 and Table 2). The axoneme of the *fap20ΔC* partially retained the
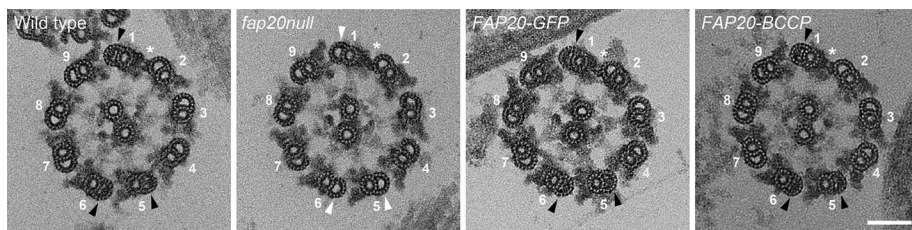
FIGURE 3: Ultrastructural defects of the *fap20null* axoneme. Cross sections of Epon-embedded axonemes of wild type, *fap20null*, and rescued strains. The 1–2 bridge (asterisks) was used to determine the position of DMT1. The beak structures contained in DMT1, 5, and 6 are indicated with arrowheads. The beak structures were completely missing in the axoneme of *fap20null* and restored in those of rescued strains. Bar, 50 nm. See Table 1 for quantitative analysis of the beak loss.

structures (Table 2), consistent with its mixed motility phenotype (Supplemental Video S3). The structures were restored in the axonemes of the rescued strains, *FAP20-GFP* and *FAP20-BCCP* (Figure 3 and Table 2), demonstrating the necessity of FAP20 for their formation. Further analysis of thin-section samples is given later.

FAP20 localizes along the entire length of all DMTs

Given that the FAP20 mutant axoneme lacked the beak structures, we examined the localization of FAP20 by immunofluorescence (Figure 4A) to compare it with proximal, DMT-specific localization of beak structures (Hoops and Witman, 1983; Nicastro et al., 2011; Pigino et al., 2012). FAP 20 antibody clearly labeled the entire length of wild-type flagella in nucleoflagellar apparatuses. Such labeling was absent in the *fap20null* flagella. This result was verified by the rescued strains, *FAP20-GFP* (Figure 4B), *FAP20-BCCP* (Supplemental Figure S4B), and *FAP20-3xHA* (unpublished data). To investigate whether all nine DMTs contain FAP20 protein, we frayed the *sup-pf1 FAP20-GFP* axonemes by protease and ATP treatment. To ensure that the axonemes frayed well, we used a double mutant with a mutant of outer arm dynein, *sup-pf1* (Huang et al., 1982; Porter et al., 1994; Mitchell et al., 2004), since its axonemes exhibit enhanced sliding efficiency (our unpublished observation). FAP20-GFP clearly localized to all nine DMTs of the frayed axoneme (Figure 4C). These observations suggest that FAP20 is not a component of the beak structure itself.

FAP20 is tightly associated with DMTs

To examine the relationship between FAP20 and known axonemal structures, we analyzed the axonemes of several representative axonemal mutants with FAP20 antibody (Figure 5A and Supplemental Table S1). FAP20 is present at wild-type levels in mutants affecting

the assembly of the radial spokes (*pf14*), the central pairs (*pf18*), the beak structures (*mbo1*, *mbo2*, *mbo3*), the outer dynein (*oda1*), the inner dyneins (*ida2*, *ida5*), and the DRC (*ida6*, *pf2*, *pf3*, *sup-pf3*, *sup-pf4*, *sup-pf5*). Therefore FAP20 must assemble in the axoneme independently of these known structures.

We next checked the protein levels of known axonemal structures in the FAP20 mutants. The proteins of the radial spokes (RSP1), the outer dynein (IC2), the inner dyneins (IC140, p28 and centrin), the nexin–DRC (N-DRC; DRC2, DRC4, DRC7), and the PF ribbon (Rib72) appeared at the wild-type amount in the FAP20 mutants (Figure 5B). The MBO2p, which is required for assembly of beaks in DMTs 5 and 6 (Tam and Lefebvre, 2002), was also unaltered. In contrast, two DMT proteins, tektin (Norrander et al., 1996; Yanagisawa and Kamiya, 2004) and PACRG (Dawe et al., 2005; Ikeda et al., 2007), were reduced in the FAP20 mutants, implying FAP20-dependent assembly on the DMT.

To further investigate FAP20's association with DMTs, we fractioned the axonemes by several treatments. Treatment with 0.6 M KCl, which removes most dynein arms but leaves DMTs intact, did not solubilize FAP20 (Figure 5C), indicating that FAP20 is tightly associated with DMTs. We then treated axonemes with increasing concentrations of Sarkosyl as previously described (Witman et al., 1972; Figure 5C). At concentrations of 0.1–0.2%, which solubilize the central pair and portions of B-tubules, FAP20 remained in the pellet, confirming the protein as a structural component of DMTs. At a concentration of 0.3%, which yields intact A-tubules with remnants of B-tubules attached at the junctions, about one-third of the FAP20 remained in the pellet. At high concentrations (0.5–0.7%), which solubilize the A-tubule, leaving the PF ribbon, FAP20 was completely solubilized. Tektin and PACRG exhibited extraction patterns quite similar to that of FAP20, supporting the notion of proximity of these three proteins on the DMT.

FAP20 is a component of the IJ

To further investigate FAP20 localization, we performed detailed structural analyses of DMTs. We first averaged cross-sectional images of embedded axonemes to identify missing structure(s) in the mutant DMTs (Figure 6, A–D). Because FAP20 localized along the length of all nine DMTs (Figure 4C), we included all DMTs except those with beak structures for averaging. The B-tubule of the wild-type DMT is composed of 10 tubulin PFs, and one smaller subunit

Strain (n)	1+, 5+, 6+	1+, 5+, 6–	1+, 5–, 6+	1+, 5–, 6–	1–, 5–, 6–
Wild type (12)	1.00	0.00	0.00	0.00	0.00
mbo1 (10)[a]	0.00	0.00	0.10	0.90	0.00
fap20null (47)	0.00	0.00	0.00	0.00	1.00
fap20ΔC (60)	0.07	0.02	0.03	0.05	0.83
FAP20-GFP (22)	0.95	0.05	0.00	0.00	0.00
FAP20-BCCP (13)	1.00	0.00	0.00	0.00	0.00

Only proximal sections with the 1–2 bridge were used for the analysis. The numbers 1, 5, and 6 refer to positions of DMTs in Figure 3, and + and – indicate the presence and absence of the beak structures in the specified DMTs, respectively.
[a]From Segal et al. (1984).

TABLE 2: Quantitative analysis of patterns of beak structures.
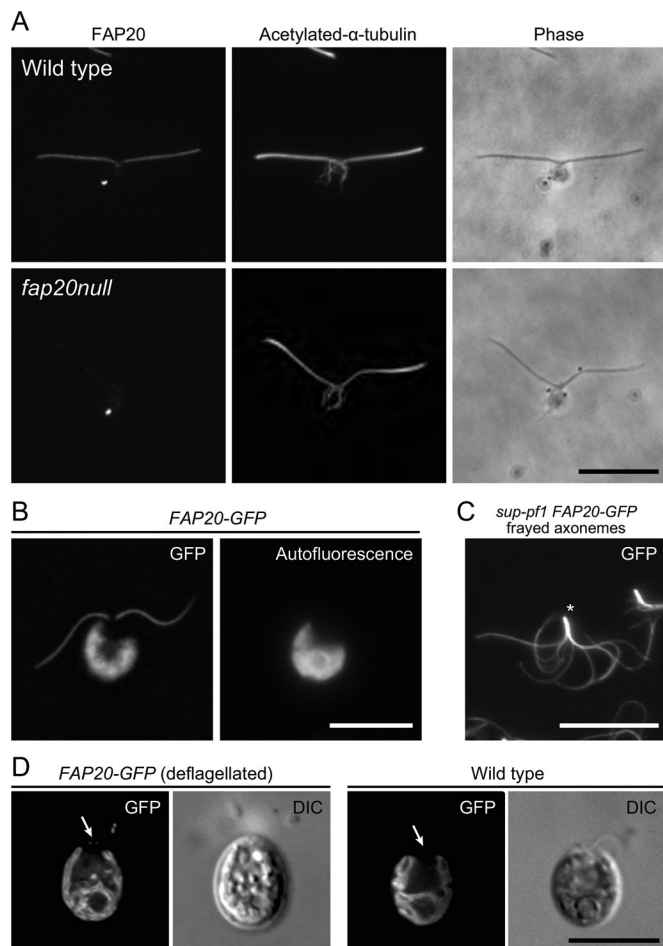
FIGURE 4: FAP20 localizes along the entire length of flagellum and is present in all nine DMTs. (A) Immunofluorescence microscopy of nucleoflagellar apparatus (NFA) shows that FAP20 is evenly distributed along the entire length of wild-type flagella, but there is no signal in *fap20null* flagella. Acetylated α-tubulin was used to show the position of flagella. (B) Fluorescence image of the rescued strain *FAP20-GFP*. The FAP20-GFP signal is evenly distributed along the entire length of flagella. (C) The axonemes of *sup-pf1 FAP20-GFP* strain, frayed by treatment with ATP and a protease, show that FAP20-GFP localizes to all nine DMTs. The base of the axoneme is resistant to the protease and remains connected (asterisk). (D) Confocal images of a deflagellated *FAP20-GFP* cell and a wild-type cell with flagella. The FAP20-GFP signal remains on the basal bodies as two discrete dots after deflagellation. There is no GFP signal on the wild-type flagella and the basal bodies. Horseshoe-shaped fluorescence in the cell bodies (B and D) is autofluorescence of the chloroplast. Bars, 10 μm.

connects between the A- and B-tubules. This smaller subunit is called the IJ and is proposed to be composed of nontubulin protein(s) (Figure 6A, black arrow; Nicastro *et al.*, 2011). Strikingly, the *fap20null* DMT lacked the smaller subunit (Figure 6B, white arrow). Loss of the smaller subunit was restored in the rescued strains (Figure 6, C and D, black arrows).

We next determined FAP20 localization by cryo–electron tomography using the streptavidin-labeling method (Oda and Kikkawa, 2013). We made a strain expressing FAP20 protein fused to a BCCP tag (Figures 1D and 2B). Biotinylation of the BCCP tag in the *FAP20-BCCP* axonemes was confirmed by Western blot analysis with peroxidase-labeled streptavidin (Supplemental Figure S4A).

Accessibility of the tag inside the axoneme was tested by labeling intact axonemes with a fluorescent streptavidin (Supplemental Figure S4B). For better visualization of the BCCP tag in cryo–electron tomography, we enlarged the tag by three-step treatments with streptavidin, biotinylated cytochrome C, and streptavidin (Oda *et al.*, 2014). The enlarged tag was clearly localized to the IJ on comparing averaged subtomograms of the *FAP20-BCCP* and wild-type DMTs (Figure 6, E and F). These observations unambiguously demonstrated that FAP20 is a bona fide IJ protein.

To verify whether the amount of FAP20 on DMTs is sufficient to form the IJ, we estimated it by comparing the fluorescence intensity of FAP20-GFP in the axoneme with that of GFP-tagged RSP3, a subunit of the radial spokes. Introduction of a GFP-tagged RSP3 gene restored the radial spokes to the axoneme (Supplemental Figure S5A) and rescued the paralyzed phenotype of an RSP3 mutant, *pf14* (Supplemental Figure S5B). Fluorescence intensity of FAP20-GFP in flagella was about three times higher than that of RSP3-GFP (Supplemental Figure S5, C and D). Previous biochemical analysis revealed that there are two radial spokes within a 96-nm longitudinal repeat of DMT, and each spoke has two or four RSP3 molecules (Yang *et al.*, 2006; Diener *et al.*, 2011; Oda *et al.*, 2014). There should be four or eight RSP3-GFP proteins per 96 nm of DMT. Using RSP3-GFP intensity as the reference, there should be roughly 12 or 24 FAP20-GFP proteins per 96 nm of DMT, which is equivalent to one FAP20-GFP protein per 8 or 4 nm of DMT. The abundance of FAP20 seemed sufficient for forming the IJ continuously along the length of the DMT.

Assembly and turnover of FAP20 in dikaryon flagella

Flagellar assembly and maintenance require continuous transport of components to the tips by intraflagellar transport (IFT; Qin *et al.*, 2004; Hou *et al.*, 2007; Ahmed *et al.*, 2008; Wren *et al.*, 2013). Dikaryon studies show that the inner arm dyneins, the radial spokes, and the DRC are delivered to the tips, where they are assembled into the axoneme (Johnson and Rosenbaum, 1992; Piperno *et al.*, 1996; Bower *et al.*, 2013). To examine whether FAP20 is transported by IFT to the flagellar tip for assembly, we mated *FAP20-GFP* gametes with both *fap20null* and wild-type gametes and observed dikaryons for the emergence of FAP20-GFP in the unlabeled flagella. In the dikaryons formed by *FAP20-GFP* and *fap20null* gametes, FAP20-GFP first appeared in the base of the *fap20null* flagella and gradually spread to the tip (Figure 7A). In the dikaryons formed by *FAP20-GFP* and wild-type gametes, no FAP20-GFP signal was observed in the wild-type flagella, indicating that in the presence of endogenous FAP20, no additional protein can be incorporated into the axoneme, and the turnover rate of FAP20 is very slow (Figure 7B). Taken together, these results hint that FAP20 is not transported into flagella by IFT but instead enters the flagella through diffusion and binds to the axoneme proximally to distally.

Localization of FAP20 on the basal bodies

FAP20 was also identified as a basal body protein through proteomic analysis (Keller *et al.*, 2005). In live, deflagellated *FAP20-GFP* cells, GFP signals were clearly visible as two discrete dots at the basal bodies (Figure 4D). The GFP signals at the basal bodies were continuous with the flagellar axonemes in the flagellated cells (Figure 4B). To confirm the localization, we also analyzed the cell bodies of IFT and basal body mutants by Western blot (Supplemental Figure S3). FAP20 is present at wild-type levels in *bld1* cells, which have normal basal bodies but cannot produce flagella because of the absence of IFT (Brazelton *et al.*, 2001; Deane *et al.*,
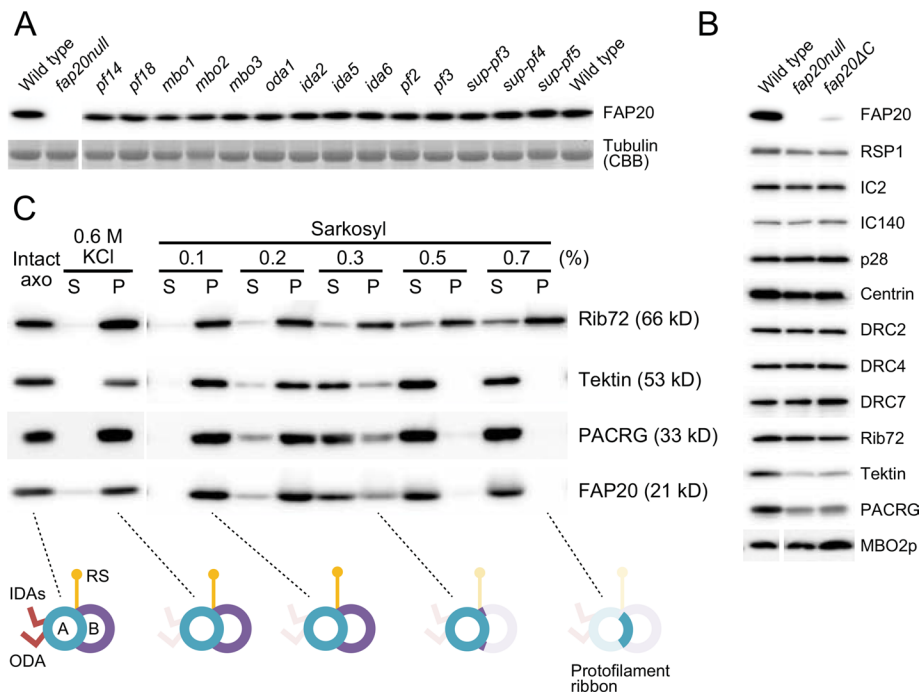
FIGURE 5: FAP20 is tightly associated with the DMT. (A) Western blot analysis of axonemes from a variety of flagellar mutants with FAP20 antibody. Coomassie-stained bands of tubulins were used as a loading control. Structures missing in each mutant are described in the text and Supplemental Table S1. (B) Western analysis of axonemes from wild type and FAP20 mutants with antibodies against a variety of axonemal proteins. Two DMT components, tektin and PACRG, are reduced in the *dmj1* axonemes. (C) Biochemical fractionation of the axonemes. The wild-type axonemes were extracted with 0.6 M KCl or various concentrations of Sarkosyl. Supernatant (S) and precipitate (P) after centrifugation were analyzed by Western blot with Rib72, tektin, PACRG, and FAP20 antibodies. Tektin, PACRG, and FAP20 exhibited a similar pattern of extraction. Rib72, a component of the PF ribbon that remains after 0.7% Sarkosyl extraction, was used as a control. Representative structures that remain in precipitates under each extraction condition are illustrated below the blots.

2001). In contrast, FAP20 protein was dramatically reduced in *bld10* cells, which completely lack the basal bodies (Matsuura *et al.*, 2004). FAP20 protein was also greatly reduced in *bld2* cells, which have short, singlet MTs instead of triplets in its basal bodies (Goodenough and St. Clair, 1975; Dutcher *et al.*, 2002). These results suggest that association of FAP20 to the basal bodies requires integrity of the MT structures.

Morpholino knockdown of Gtl3/FAP20 caused a ciliary phenotype in zebrafish

Vertebrate homologues of FAP20, GTL3/C16orf80, are highly expressed in the testis and other ciliated tissues (Rijkers and Ruther, 1996) and found in cilia proteomes (Ostrowski *et al.*, 2002). To test whether GTL3/C16orf80 has a conserved function in vertebrate cilia, we performed morpholino-mediated knockdown experiments in zebrafish embryos. The *gtl3*-knockdown fish showed a curved body axis (Supplemental Figure S6A), short somite length (Supplemental Figure S6, B and C), and defective heart-looping orientation (Supplemental Figure S6D). These phenotypes are consistent with ciliary dysfunction in zebrafish (Malicki *et al.*, 2011). We also examined the cilia in the Kupffer's vesicles in the *gtl3*-knockdown fish by immunostaining with an acetylated-tubulin antibody. Both the number and the length of cilia were reduced compared with the control morpholino fish (Supplemental Figure S6, E–G), implying that GTL3 may be important for assembly or stability of cilia in zebrafish.

DISCUSSION

In this study, we demonstrated that a highly conserved flagellar protein, FAP20, is an IJ protein of DMTs. This is the first report to locate a component of DMTs at the ultrastructural level. Through mutant analysis, we showed that FAP20 protein is essential for both stability of the axoneme and a planar asymmetrical waveform.

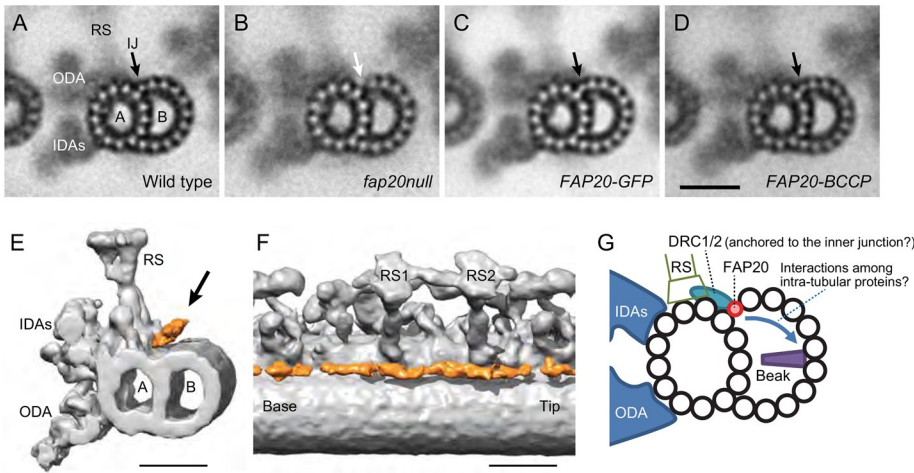### FAP20 is an IJ protein of axonemal DMTs

High-resolution cryo–electron tomography analyses showed that the IJ of DMTs comprises smaller, nontubulin subunits (Nicastro *et al.*, 2011; Pigino *et al.*, 2012). We showed that the FAP20 mutant lacks the nontubulin subunit of the IJ (Figure 6B) and the tagged FAP20 localized to the IJ (Figure 6, E and F). These two observations clearly demonstrate that FAP20 is a component of the IJ. The stoichiometry of FAP20 to RSP3 supports the notion that FAP20 binds to the DMT with 8- or 4-nm periodicity (Supplemental Figure S5C). This also means that FAP20 is one of the most abundant proteins in the DMT besides tubulins. Two DMT proteins, tektin and PACRG, were reduced in the FAP20 mutant (Figure 5B) and cofractionated with FAP20 in the biochemical analyses (Figure 5C), suggesting that these proteins may interact with FAP20. Based on our calculation, one or two FAP20 proteins contribute 21 or 42 kDa/8 nm, which is too small to be the sole component of the IJ, since the size of the IJ is comparable to that of tubulin PFs (~100 kDa/8 nm). Thus tektin (58 kDa) and PACRG (33 kDa) may colocalize with FAP20 to form the IJ. We rarely observed any open B-tubule in the mutant axoneme, suggesting that the reduced amount of these proteins may partially maintain the IJ or rigidity of the outer junction, and the B-tubule wall may be enough to maintain the shape of the B-tubule.

The integrity of the IJ is important for stability of the axoneme

Interdoublet connections have been reported to be mediated by the N-DRC (Heuser *et al.*, 2009). A structural study showed that there is a hole along the IJ at 96-nm intervals in the wild-type axoneme, and the hole is filled in the axoneme of N-DRC mutants *pf3* and *ida6* (Nicastro *et al.*, 2011). The mutated proteins, DRC1 and DRC2, compose the base plate that facilitates the attachment of the N-DRC to the A-tubule and extends to the IJ (Heuser *et al.*, 2009). This raises the possibility that DRC1, DRC2, or their interacting protein(s) are anchored to the IJ (Figure 6G), affecting packing of the IJ proteins to form the hole (Nicastro *et al.*, 2011). In our previous study, tektin, a putative interacting protein of FAP20, was reduced in the *pf3* and *ida6* axonemes (Yanagisawa and Kamiya, 2004), supporting the notion of proximity between the DRC proteins and the IJ proteins. Loss of the IJ in the FAP20 mutant may weaken the anchorage of the N-DRC and destabilize the interdoublet connection. Indeed, the axoneme of the FAP20 mutant is liable to be disintegrated during beating (Figure 2, D and E).

FIGURE 6: FAP20 is an IJ protein. (A–D) The *fap20null* axoneme is defective in the IJ between A- and B-tubules. Images of DMTs in cross sections of Epon-embedded axonemes were averaged. DMT1, 5, and 6 were excluded from the analyses. The number of DMT images used for the averaging is 22, 22, 65, and 34, respectively, for wild type, *fap20null*, *FAP20-GFP*, and *FAP20-BCCP*. IDAs, inner dynein arms; IJ, inner junction (arrows); ODA, outer dynein arm; RS, radial spoke. (A) The wild-type B-tubule is composed of 10 tubulin PFs and one smaller, nontubulin subunit at the IJ (B) The DMT of the *fap20null* clearly lacks the nontubulin subunit. (C, D) The nontubulin subunits are restored in the rescued strains. Bar, 20 nm. (E, F) FAP20 localized to the inner junction (IJ) of the DMT. (E, F) Wild-type and *FAP20-BCCP* axonemes were labeled by an enhanced streptavidin-label method. The position of the streptavidin–cytochrome C label (orange) in the DMT was visualized by comparing averaged subtomograms of the two strains. (E) Cross-sectional view from the base of the axoneme. (F) Lateral view from a direction indicated by an arrow in E. Bars, 25 nm. (G) Model of FAP20 localization and functions. FAP20 localizes to the IJ between A- and B-tubules and stabilizes the DMT. N-DRC components, DRC1/2, or its associated proteins may extend to the IJ and be anchored by FAP20. In DMT1, 5, and 6, FAP20 may work as a scaffold for intratubular proteins to produce the beak structures.

ever, FAP20 is neither a beak component nor a determinant to specify DMTs with beaks; FAP20 itself localized uniformly along the length of all nine DMTs (Figure 4C), and the amount of FAP20 was unaffected in the axonemes of *mbo* mutants, which partially lack the beak structures (Figure 4A). Instead, FAP20 may function just as a scaffold for assembly of the beaks in DMTs specified by unknown factors (Figure 6G).
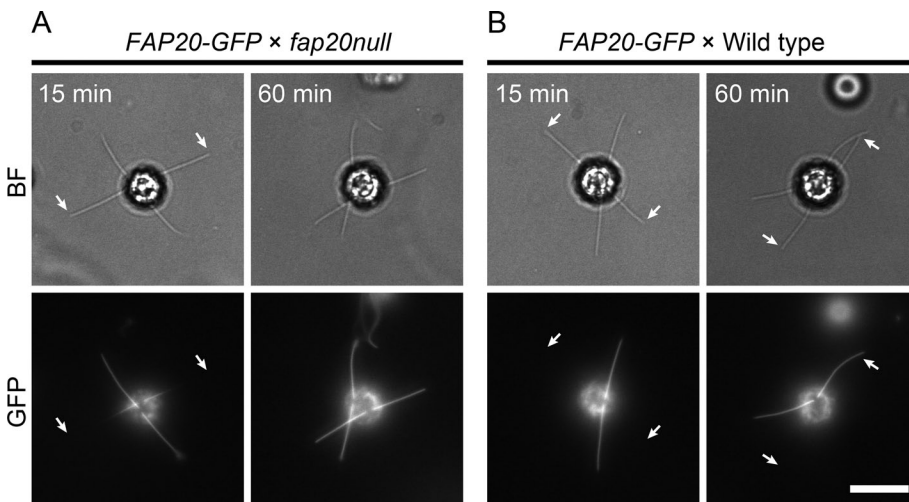
The underlying mechanism for generating the widely used planar asymmetrical beating of cilia or flagella is unknown. The beak structures required for asymmetrical waveform are found only in *Chlamydomonas*. It is possible that functionally equivalent structures are present in other organisms, given the following evidence: 1) MBO2p/CCDC146, the mutated protein of *Chlamydomonas mbo2* mutant, is conserved among organisms with flagella or cilia (Tam and Lefebvre, 2002); and 2) knockdown of FAP20/BUG22 in *Paramecium* causes symmetrical ciliary beating (Laligne *et al.*, 2010) similar to that of the *Chlamydomonas* mutant. Further functional studies of these proteins in other organisms are necessary to confirm whether a conserved mechanism is used to generate planar asymmetrical beating of cilia or flagella.

The IJ may function as a scaffold for assembly of beak structures

The FAP20 mutant completely lacks the doublet-specific beak structures (Figure 3), which are localized in the proximal portion of the axoneme and related to the direction of the bending. How-

FAP20 has a novel mode of assembly

In the dikaryon analyses (Figure 7), we found that FAP20 is assembled into the mutant axoneme from base to tip. This is opposite to the tip-to-base assembly of other axonemal components (Johnson and Rosenbaum, 1992; Piperno *et al.*, 1996; Bower *et al.*, 2013). The unique axonemal assembly pattern of FAP20 may reflect that it is a component of the DMT itself and involved in the assembly of intratubular beak structures. It will be interesting to examine whether IFT is involved in the flagellar entry of FAP20.

This unusual mode of assembly provides an explanation for several inconsistent results reported for tagged FAP20 localization in different organisms. In *Trypanosoma* (Hodges *et al.*, 2011), FAP20 localized along the entire length of the axoneme, consistent with our observation (Figure 4, A and B, and Supplemental Figure S4B). In contrast, the tagged FAP20 only localized to the proximal portion of the cilia in *Paramecium* (Laligne *et al.*, 2010), cultured mammalian cells (Ishikawa *et al.*, 2012), and *Chlamydomonas* (Meng *et al.*, 2013). In the these three studies, tagged transgenes were expressed in the presence of endogenous FAP20/GTL3 or the expression levels were lower than that of wild type. As we show in this study, FAP20 is incorporated into the axoneme from base

FIGURE 7: FAP20 is assembled into the flagella from base to tip. *FAP20-GFP* gametes were mated with both *fap20null* (A) and wild-type (B) gametes and dikaryons observed for the emergence of FAP20-GFP in the unlabeled flagella. Bright-field (BF) and GFP fluorescence images of dikaryons were recorded at 15 and 60 min after mixing. (A) FAP20-GFP fluorescence first appeared at the base of the *fap20null* flagella and gradually extended to the tip. (B) FAP20-GFP was not incorporated into wild-type flagella. Arrows indicate positions of flagellar tips.

to tip and with very low turnover rate (Figure 7). Thus it is reasonable to observe that the tagged proteins localized only to the proximal portion of the axonemes in these studies because the expression level was low or not up-regulated upon growth of the axonemes.

Basal body localization of FAP20 family proteins

FAP20 was identified as a basal body component in a previous proteomic study (Keller et al., 2005). The basal bodies are arranged in a V shape in which the proximal ends are closely associated (Ringo, 1967). In contrast to the fused-single-dot staining observed with antibodies against proximal-end proteins (Matsuura et al., 2004; Nakazawa et al., 2007), FAP20 localized to the basal bodies as two discrete dots in deflagellated cells. These two dots were on the mature basal bodies but not the pro–basal bodies because the dots were continuous with the FAP20 staining on the axonemes in flagellated cells. The distance between the two dots was ~0.8 μm, corresponding to the distance between the distal ends. FAP20 in the basal body is not essential for templating the axoneme since the FAP20 mutants exhibit no abnormality in flagellar assembly (Figure 2A). These observations suggest that FAP20 in the basal bodies may be localized to the distal ends, which are formed by DMTs instead of triplet MTs and are not essential for templating the axoneme.

FAP20 homologues are annotated as members of the domain of unknown function (DUF667) family in protein family databases (e.g., http://pfam.sanger.ac.uk/). Of interest, several proteins contain DUF667. One of the proteins, WDR90, is highly conserved among organisms with cilia and flagella. WDR90 is not in ciliary or flagellar proteomes but is instead found in the basal body proteome (Keller et al., 2005) and annotated as proteome of centriole 16 (POC16). WDR90/POC16 contains one DUF667 domain in its N-terminus, followed by a large C-terminal domain containing multiple WD40 repeats. A structural study of the basal bodies revealed that the IJ between the triplet A- and B-tubules scaffolds a large structure called the Y-shaped linker (Li et al., 2012). WDR90/POC16 may form both the IJ and part of the linker in the triplet MT.

FAP20 may play a conserved role in modifying the functionality of MTs

In this article, we showed that FAP20 forms the IJ of DMTs. The IJ seems to function as an essential hub for protein interactions in the DMT; the IJ likely anchors the N-DRC and scaffolds the intra–B-tubular beak structure. We propose that the flagellar stability and motility defects of FAP20 mutants are caused by the dysfunction/loss of these structures. Recently, a Drosophila FAP20 mutant was reported to be defective in tubulin polyglycylation in sperm MTs (Mendes Maia et al., 2014). The IJ may work as a guide for tubulin modification enzymes. Moreover, FAP20 is also present in nonmotile primary cilia, which lack motility-specific proteins, including DRC subunits (Ishikawa et al., 2012). FAP20 likely forms the IJ of DMTs and might mainly strengthen the rigidity of axonemes in the primary cilia. Further studies are required to evaluate the role of the IJ in mechanical properties of DMTs.

MATERIALS AND METHODS

Strains and culture conditions

Chlamydomonas reinhardtii strains used for this study are listed in Supplemental Table S1. Cells were cultured on Tris-acetate-phosphate medium (TAP) plates with 1.5% agar or in liquid TAP with constant aeration at 22 or 25°C with a 12:12 h light:dark cycle. Gametes for dikaryon analyses were prepared by shaking cells in M-N (Sager and Granick minimum medium without nitrogen source) liquid medium for 4 h under illumination.

Isolation and mapping of FAP20 mutants

The first allele, dmj1-1, was isolated from a library of motility mutants generated by insertional mutagenesis using a marker plasmid, pSI103 (Sizova et al., 2001). The mutation was not linked to the marker plasmid and thus was mapped to the FAP20 gene by AFLP analysis (Kathir et al., 2003). The second allele, dmj1-2, was isolated from a library of motility mutants generated by ultraviolet (UV) mutagenesis. The third allele, RL-11, was previously described (Nakamura, 1981). Both dmj1-2 and RL-11 were identified as FAP20 mutants by sequencing of the FAP20 gene. The fourth allele, dmj1-3, was screened from a phototaxis-defective mutant library created by insertional mutagenesis of a hygromycin B–resistant gene (Berthold et al., 2002). The mutation was mapped to the FAP20 gene by restriction enzyme site-directed amplification PCR (Gonzalez-Ballester et al., 2005). Oligonucleotide primers used for amplification and sequencing of the FAP20 gene are listed in Supplemental Table S2. Each mutant was backcrossed at least twice for the experiments reported in this study.

Antibodies

The full-length FAP20 cDNA was amplified by reverse transcription-PCR with primers FAP20-BglNd-F and FAP20-Xho-R. The truncated FAP20 cDNA was amplified with primers FAP20-BglNd-F and FAP20-TR-Xho-R. The full-length product was digested with NdeI and XhoI and cloned into pET24a (Merck, Darmstadt, Germany) to produce FAP20full-His. Both the full-length and the truncated products were digested with BglII and XhoI and cloned between BamHI and XhoI sites of pGEX6P2 (GE Healthcare, Little Chalfont, United Kingdom) to produce glutathione S-transferase (GST)–FAP20full and GST-FAP20ΔC20aa, respectively. Each of the three plasmids was transformed into BL21 (DE3). The expression of the recombinant proteins was induced by adding 1 mM isopropyl-β-D-thiogalactoside into a logarithmically growing culture. Almost all of the expressed proteins were contained within inclusion bodies. The inclusion bodies were purified as previously described (Yanagisawa and Kamiya, 2004). FAP20full-His was used to immunize two rabbits. The antibodies were affinity purified using GST-FAP20full or GST-FAP20ΔC20aa blotted onto polyvinylidene difluoride membranes. Sequences of the primers used for the plasmid constructions are listed in Supplemental Table S2. Other antibodies used in this study are listed in Supplemental Table S3.

Isolation and biochemical fractionation of axonemes

Chlamydomonas cells were deflagellated with dibucaine-HCl (Wako Pure Chemical Industries, Tokyo, Japan), and axonemes were collected by centrifugation (Witman et al., 1978). The flagella were demembranated with 1% Nonidet P-40 in HMDEK buffer (30 mM 4-(2-hydroxyethyl)-1-piperazineethanesulfonic acid–NaOH, pH 7.2, 5 mM MgCl$_2$, 1 mM dithiothreitol, 1 mM ethylene glycol tetraacetic acid, 50 mM CH$_3$COOK, 1× protease inhibitor cocktail [Nacalai Tesque, Kyoto, Japan]). Biochemical fractionation of the axonemes was performed as previously described (Witman et al., 1972; Yanagisawa and Kamiya, 2004).

Plasmid constructions

To make FAP20 constructs with tags, an ~4.5-kb fragment containing the FAP20 gene was amplified from Chlamydomonas genomic DNA using primers FAP20-gDNA-F and FAP20-gDNA-R. The PCR product was cloned into the EcoRV site of pBluescript II to create the construct pBS-FAP20. A unique EcoRV site was introduced before the stop codon by PCR amplification of the entire plasmid with primers FAP20-gDNA-C-ERV-F and FAP20-gDNA-C-ERV-R. The

PCR product with 16-base cohesive ends was transformed into DH5α to make the construct pBS-FAP20-C-ERV. A GFP tag was cut out with *Bam*HI from pCrGFP (Fuhrmann *et al*., 1999) and blunted with Klenow. A 3xHA tag was cut out with *Nru*I and *Sca*I from p3xHA (Silflow *et al*., 2001). Each of the two tag fragments was ligated into the *Eco*RV site of pBS-FAP20-C-ERV. A BCCP tag was amplified from pGenD-LC2-BCCP (Furuta *et al*., 2009) using primers FAP20-BCCP-F and FAP20-BCCP-R and cloned into the *Eco*RV site of pBS-FAP20-C-ERV using In-Fusion HD Cloning Kit (Clontech, Mountain View, CA). Each of the three FAP20 constructs was linearized with *Eco*RI and cotransformed with pSI103 into the *dmj1-1* cells by electroporation to produce the rescued strains *dmj1-1*::FAP20-GFP, *dmj1-1*::FAP20-3xHA, and *dmj1-1*::FAP20-BCCP. Sequences of the primers used for the plasmid constructions are listed in Supplemental Table S2.

Flagella length measurement
Cells were fixed with 2× Lugol's iodine and placed in 4°C until the end of the experiment. The cells were observed by an Axioplan phase contrast microscope (Carl Zeiss, Oberkochen, Germany). Still images were taken with a Phantom Miro-eX2 (Vision Research, Wayne, NJ), and the length of a single flagellum from each cell was measured using the ImageJ (Schneider *et al*., 2012) segmented line tool.

Assessment of flagellar motility
For waveform analyses, cells were observed by an Axioplan phase contrast microscope or a BX51 dark-field microscope (Olympus, Tokyo, Japan). To prevent photoshock, a red filter was used. The filter was removed to induce waveform change in wild-type cells. Movies for waveform analysis were taken with a Phantom Miro-eX2 or an EoSens MC1362 (Mikrotron, Unterschleissheim, Germany) at either 600 or 1000 fps. To trace the waveforms, the movies were imported into ImageJ and trimmed to 10 frames with equal time elapsed between frames of a given set. Shapes of the flagella were traced over a lowered opacity using Illustrator (Adobe, San Jose, CA). For measurement of swimming velocity, cells were observed by a dark-field microscope and movies were recorded as described at 30 fps. Swimming velocity of the cells was measured using the MTrack2 plug-in (Klopfenstein and Vale, 2004) of ImageJ.

Immunofluorescence microscopy
Nucleoflagellar apparatus prepared as previously described (Taillon and Jarvik, 1995) was fixed with 2% formaldehyde for 10 min at room temperature, followed by treatment with cold acetone and methanol (–20°C). Fixed samples were immunostained as previously described (Sanders and Salisbury, 1995). Samples were observed by an IX70 fluorescence microscope (Olympus) with an ORCA-R2 charge-coupled device (CCD) camera (Hamamatsu Photonics, Shizuoka, Japan).

Live-cell imaging of the GFP-tagged strain
Live cells of the *dmj1-1*::FAP20-GFP were observed by an IX70 microscope as described or an IX81 microscope (Olympus) equipped with a disk scanning unit and iXon electron-multiplying CCD camera (Andor Technology, Belfast, United Kingdom). Fluorescence intensities of flagella were measured using ImageJ.

Reactivation and disintegration of isolated axonemes
To analyze the stability of the *dmj1-1* axoneme, isolated axonemes were reactivated in HMDEK buffer containing 0.1 mM ATP without proteases. Motility and disintegration of the axonemes were

observed by a dark-field microscope and recorded using a MC-681SPD high-sensitive CCD camera (Texas Instruments, Dallas, TX). To observe FAP20-GFP fluorescence on the DMTs, the isolated axoneme from *dmj1-1*::FAP20-GFP was adsorbed on a slide and treated with 1 μg/ml Type XXIV bacterial proteinase (Sigma-Aldrich, St. Louis, MO) and 1 mM ATP in HMDEK-PI (HMDEK without protease inhibitors) buffer for 30 s at room temperature. GFP fluorescence was observed as described.

Thin-section electron microscopy
Thin-section electron microscopy of the axonemes was performed as previously described (Huang *et al*., 1979). The cacodylate buffer in the method was substituted by 50 mM Na-phosphate, pH 7.0. The samples were observed by a JEM-3100FEF transmission electron microscope (JEOL, Tokyo, Japan) equipped with TemCam-F416 (TVIPS, Gauting, Germany). Images were recorded at 300 keV, with ~3-μm defocus, at a magnification of ×82,100 and a pixel size of 1.9 Å. Cross-sectional images in which the PFs were clearly visible were selected and used for averaging of DMTs. Alignment and averaging of DMTs were conducted using custom Ruby-Helix scripts (Metlagel *et al*., 2007) and the align2d program of EMAN (Ludtke *et al*., 1999).

Assessment of the BCCP-tagged strain
Biotinylation of the FAP20-BCCP in the *dmj1-1*::FAP20-BCCP axonemes was confirmed by Western blotting with streptavidin–horseradish peroxidase (Thermo Fisher Scientific, Waltham, MA). Accessibility of the BCCP tag in the intact axoneme was assessed using fluorescence-labeled streptavidin. Demembranated axonemes were loaded to a flow cell and blocked with 1% bovine serum albumin (BSA) in HMDEK buffer. Then the flow cell was perfused with streptavidin–Alexa Fluor 546 (Life Technologies, Carlsbad, CA) diluted 1:1000 in the same buffer and washed with the buffer alone. Samples were observed by an IX70 fluorescence microscope as described.

Enhanced streptavidin labeling of the axonemes
Demembranated axonemes were incubated with 0.05 mg/ml streptavidin (Wako Pure Chemical Industries) for 15 min at 4°C in HMDEK buffer. Axonemes were washed five times with HMDEK buffer and incubated with 0.05 mg/ml biotinylated cytochrome C for 15 min at 4°C in the presence of 1 mg/ml BSA and 0.1 mg/ml unlabeled cytochrome C. Axonemes were washed five times with HMDEK again and incubated with 0.05 mg/ml streptavidin for 15 min at 4°C. Labeled axonemes were separated from unbound streptavidin by centrifugation and were resuspended in HMDEK buffer at a concentration of 0.02 mg/ml and mixed with equal amount of 15-nm colloidal gold suspension conjugated with BSA (Aurion, Wageningen, Netherlands). Home-made holey carbon grids were glow discharged and coated with 20-nm colloidal gold (BBInternational, Cardiff, United Kingdom). Suspended axonemes plus colloidal gold (5 μl) was loaded onto the grids and plunge frozen in liquid ethane at –180°C with an automated plunge-freezing device, EM GP (Leica Microsystems, Wetzlar, Germany). Images were acquired and processed as previously described (Oda and Kikkawa, 2013) with little modification. The details are described in the Supplemental Methods.

REFERENCES

Ahmed NT, Gao C, Lucker BF, Cole DG, Mitchell DR (2008). ODA16 aids axonemal outer row dynein assembly through an interaction with the intraflagellar transport machinery. J Cell Biol 183, 313–322.

Berthold P, Schmitt R, Mages W (2002). An engineered *Streptomyces hygroscopicus* aph 7″ gene mediates dominant resistance against hygromycin B in *Chlamydomonas reinhardtii*. Protist 153, 401–412.

Bower R, Tritschler D, Vanderwaal K, Perrone CA, Mueller J, Fox L, Sale WS, Porter ME (2013). The N-DRC forms a conserved biochemical complex that maintains outer doublet alignment and limits microtubule sliding in motile axonemes. Mol Biol Cell 24, 1134–1152.

Brazelton WJ, Amundsen CD, Silflow CD, Lefebvre PA (2001). The *bld1* mutation identifies the *Chlamydomonas osm-6* homolog as a gene required for flagellar assembly. Curr Biol 11, 1591–1594.

Dawe HR, Farr H, Portman N, Shaw MK, Gull K (2005). The Parkin co-regulated gene product, PACRG, is an evolutionarily conserved axonemal protein that functions in outer-doublet microtubule morphogenesis. J Cell Sci 118, 5421–5430.

Deane JA, Cole DG, Seeley ES, Diener DR, Rosenbaum JL (2001). Localization of intraflagellar transport protein IFT52 identifies basal body transitional fibers as the docking site for IFT particles. Curr Biol 11, 1586–1590.

Diener DR, Yang P, Geimer S, Cole DG, Sale WS, Rosenbaum JL (2011). Sequential assembly of flagellar radial spokes. Cytoskeleton (Hoboken) 68, 389–400.

Dutcher SK (1995). Flagellar assembly in two hundred and fifty easy-to-follow steps. Trends Genet 11, 398–404.

Dutcher SK, Morrissette NS, Preble AM, Rackley C, Stanga J (2002). Epsilon-tubulin is an essential component of the centriole. Mol Biol Cell 13, 3859–3869.

Euteneuer U, McIntosh JR (1980). Polarity of midbody and phragmoplast microtubules. J Cell Biol 87, 509–515.

Fuhrmann M, Oertel W, Hegemann P (1999). A synthetic gene coding for the green fluorescent protein (GFP) is a versatile reporter in *Chlamydomonas reinhardtii*. Plant J 19, 353–361.

Furuta A, Yagi T, Yanagisawa HA, Higuchi H, Kamiya R (2009). Systematic comparison of in vitro motile properties between *Chlamydomonas* wild-type and mutant outer arm dyneins each lacking one of the three heavy chains. J Biol Chem 284, 5927–5935.

Gonzalez-Ballester D, de Montaigu A, Galvan A, Fernandez E (2005). Restriction enzyme site-directed amplification PCR: a tool to identify regions flanking a marker DNA. Anal Biochem 340, 330–335.

Goodenough UW, St. Clair HS (1975). BALD-2: a mutation affecting the formation of doublet and triplet sets of microtubules in *Chlamydomonas reinhardtii*. J Cell Biol 66, 480–491.

Heuser T, Raytchev M, Krell J, Porter ME, Nicastro D (2009). The dynein regulatory complex is the nexin link and a major regulatory node in cilia and flagella. J Cell Biol 187, 921–933.

Hildebrandt F, Benzing T, Katsanis N (2011). Ciliopathies. N Engl J Med 364, 1533–1543.

Hodges ME, Wickstead B, Gull K, Langdale JA (2011). Conservation of ciliary proteins in plants with no cilia. BMC Plant Biol 11, 185.

Hoops HJ, Witman GB (1983). Outer doublet heterogeneity reveals structural polarity related to beat direction in *Chlamydomonas* flagella. J Cell Biol 97, 902–908.

Hou Y, Qin H, Follit JA, Pazour GJ, Rosenbaum JL, Witman GB (2007). Functional analysis of an individual IFT protein: IFT46 is required for transport of outer dynein arms into flagella. J Cell Biol 176, 653–665.

Huang B, Piperno G, Luck DJ (1979). Paralyzed flagella mutants of *Chlamydomonas reinhardtii*. Defective for axonemal doublet microtubule arms. J Biol Chem 254, 3091–3099.

Huang B, Ramanis Z, Luck DJ (1982). Suppressor mutations in *Chlamydomonas* reveal a regulatory mechanism for flagellar function. Cell 28, 115–124.

Ikeda K, Brown JA, Yagi T, Norrander JM, Hirono M, Eccleston E, Kamiya R, Linck RW (2003). Rib72, a conserved protein associated with the ribbon compartment of flagellar A-microtubules and potentially involved in the linkage between outer doublet microtubules. J Biol Chem 278, 7725–7734.

Ikeda K, Ikeda T, Morikawa K, Kamiya R (2007). Axonemal localization of *Chlamydomonas* PACRG, a homologue of the human Parkin-coregulated gene product. Cell Motil Cytoskeleton 64, 814–821.

Ishikawa H, Marshall WF (2011). Ciliogenesis: building the cell's antenna. Nat Rev Mol Cell Biol 12, 222–234.

Ishikawa H, Thompson J, Yates JR3rd, Marshall WF (2012). Proteomic analysis of mammalian primary cilia. Curr Biol 22, 414–419.

Johnson KA, Rosenbaum JL (1992). Polarity of flagellar assembly in *Chlamydomonas*. J Cell Biol 119, 1605–1611.

Kathir P, LaVoie M, Brazelton WJ, Haas NA, Lefebvre PA, Silflow CD (2003). Molecular map of the *Chlamydomonas reinhardtii* nuclear genome. Eukaryot Cell 2, 362–379.

Keller LC, Romijn EP, Zamora I, Yates JR 3rd, Marshall WF (2005). Proteomic analysis of isolated *Chlamydomonas* centrioles reveals orthologs of ciliary-disease genes. Curr Biol 15, 1090–1098.

Klopfenstein DR, Vale RD (2004). The lipid binding pleckstrin homology domain in UNC-104 kinesin is necessary for synaptic vesicle transport in *Caenorhabditis elegans*. Mol Biol Cell 15, 3729–3739.

Laligne C, Klotz C, de Loubresse NG, Lemullois M, Hori M, Laurent FX, Papon JF, Louis B, Cohen J, Koll F (2010). Bug22p, a conserved centrosomal/ciliary protein also present in higher plants, is required for an effective ciliary stroke in *Paramecium*. Eukaryot Cell 9, 645–655.

Li S, Fernandez JJ, Marshall WF, Agard DA (2012). Three-dimensional structure of basal body triplet revealed by electron cryo-tomography. EMBO J 31, 552–562.

Linck RW, Albertini DF, Kenney DM, Langevin GL (1982). Tektin filaments: chemically unique filaments of sperm flagellar microtubules. Cell Motility 2, 127–132.

Linck RW, Stephens RE (2007). Functional protofilament numbering of ciliary, flagellar, and centriolar microtubules. Cell Motil Cytoskeleton 64, 489–495.

Ludtke SJ, Baldwin PR, Chiu W (1999). EMAN: semiautomated software for high-resolution single-particle reconstructions. J Struct Biol 128, 82–97.

Malicki J, Avanesov A, Li J, Yuan S, Sun Z (2011). Analysis of cilia structure and function in zebrafish. Methods Cell Biol 101, 39–74.

Matsuura K, Lefebvre PA, Kamiya R, Hirono M (2004). Bld10p, a novel protein essential for basal body assembly in *Chlamydomonas*: localization to the cartwheel, the first ninefold symmetrical structure appearing during assembly. J Cell Biol 165, 663–671.

Mendes Maia T, Gogendeau D, Pennetier C, Janke C, Basto R (2014). Bug22 influences cilium morphology and the post-translational modification of ciliary microtubules. Biol Open 3, 138–151.

Meng D, Cao M, Oda T, Kikkawa M, Pan J (2013). The conserved ciliary protein Bug22 controls planar beating of *Chlamydomonas* flagella. J Cell Sci 127, 281–287.

Metlagel Z, Kikkawa YS, Kikkawa M (2007). Ruby-Helix: an implementation of helical image processing based on object-oriented scripting language. J Struct Biol 157, 95–105.

Mitchell BF, Grulich LE, Mader MM (2004). Flagellar quiescence in *Chlamydomonas*: Characterization and defective quiescence in cells carrying *sup-pf-1* and *sup-pf-2* outer dynein arm mutations. Cell Motil Cytoskeleton 57, 186–196.

Nakamura S (1981). Two different backward-swimming mutants of *Chlamydomonas reinhardtii*. Cell Struct Funct 6, 385–393.

Nakazawa Y, Hiraki M, Kamiya R, Hirono M (2007). SAS-6 is a cartwheel protein that establishes the 9-fold symmetry of the centriole. Curr Biol 17, 2169–2174.

Nicastro D, Fu X, Heuser T, Tso A, Porter ME, Linck RW (2011). Cryo-electron tomography reveals conserved features of doublet microtubules in flagella. Proc Natl Acad Sci USA 108, E845–E853.

Norrander JM, deCathelineau AM, Brown JA, Porter ME, Linck RW (2000). The Rib43a protein is associated with forming the specialized protofilament ribbons of flagellar microtubules in *Chlamydomonas*. Mol Biol Cell 11, 201–215.

Norrander JM, Perrone CA, Amos LA, Linck RW (1996). Structural comparison of tektins and evidence for their determination of complex spacings in flagellar microtubules. J Mol Biol 257, 385–397.

Oda T, Kikkawa M (2013). Novel structural labeling method using cryo-electron tomography and biotin-streptavidin system. J Struct Biol 183, 305–311.

Oda T, Yanagisawa H, Yagi T, Kikkawa M (2014). Mechano-signaling between central apparatus and radial spokes controls axonemal dynein activity. J Cell Biol 204, 807–819.

Ostrowski LE, Blackburn K, Radde KM, Moyer MB, Schlatzer DM, Moseley A, Boucher RC (2002). A proteomic analysis of human cilia: identification of novel components. Mol Cell Proteomics 1, 451–465.

Pazour GJ, Agrin N, Leszyk J, Witman GB (2005). Proteomic analysis of a eukaryotic cilium. J Cell Biol 170, 103–113.

Pigino G, Maheshwari A, Bui KH, Shingyoji C, Kamimura S, Ishikawa T (2012). Comparative structural analysis of eukaryotic flagella and cilia from *Chlamydomonas*, *Tetrahymena*, and sea urchins. J Struct Biol 178, 199–206.

Piperno G, Mead K, Henderson S (1996). Inner dynein arms but not outer dynein arms require the activity of kinesin homologue protein KHP1(FLA10) to reach the distal part of flagella in *Chlamydomonas*. J Cell Biol 133, 371–379.

Porter ME, Knott JA, Gardner LC, Mitchell DR, Dutcher SK (1994). Mutations in the SUP-PF-1 locus of *Chlamydomonas reinhardtii* identify a regulatory domain in the beta-dynein heavy chain. J Cell Biol 126, 1495–1507.

Qin H, Diener DR, Geimer S, Cole DG, Rosenbaum JL (2004). Intraflagellar transport (IFT) cargo: IFT transports flagellar precursors to the tip and turnover products to the cell body. J Cell Biol 164, 255–266.

Rijkers T, Ruther U (1996). Sequence and expression pattern of an evolutionarily conserved transcript identified by gene trapping. Biochim Biophys Acta 1307, 294–300.

Ringo DL (1967). Flagellar motion and fine structure of the flagellar apparatus in *Chlamydomonas*. J Cell Biol 33, 543–571.

Sanders MA, Salisbury JL (1995). Immunofluorescence microscopy of cilia and flagella. Methods Cell Biol 47, 163–169.

Schneider CA, Rasband WS, Eliceiri KW (2012). NIH Image to ImageJ: 25 years of image analysis. Nat Methods 9, 671–675.

Segal RA, Huang B, Ramanis Z, Luck DJ (1984). Mutant strains of *Chlamydomonas reinhardtii* that move backwards only. J Cell Biol 98, 2026–2034.

Silflow CD, LaVoie M, Tam LW, Tousey S, Sanders M, Wu W, Borodovsky M, Lefebvre PA (2001). The Vfl1 protein in *Chlamydomonas* localizes in a rotationally asymmetric pattern at the distal ends of the basal bodies. J Cell Biol 153, 63–74.

Sizova I, Fuhrmann M, Hegemann P (2001). A *Streptomyces rimosus aphVIII* gene coding for a new type phosphotransferase provides stable antibiotic resistance to *Chlamydomonas reinhardtii*. Gene 277, 221–229.

Taillon BE, Jarvik JW (1995). Release of the cytoskeleton and flagellar apparatus from *Chlamydomonas*. Methods Cell Biol 47, 307–313.

Tam LW, Lefebvre PA (2002). The *Chlamydomonas MBO2* locus encodes a conserved coiled-coil protein important for flagellar waveform conversion. Cell Motil Cytoskeleton 51, 197–212.

Witman GB, Carlson K, Berliner J, Rosenbaum JL (1972). *Chlamydomonas* flagella. I. Isolation and electrophoretic analysis of microtubules, matrix, membranes, and mastigonemes. J Cell Biol 54, 507–539.

Witman GB, Plummer J, Sander G (1978). *Chlamydomonas* flagellar mutants lacking radial spokes and central tubules. Structure, composition, and function of specific axonemal components. J Cell Biol 76, 729–747.

Wren KN, Craft JM, Tritschler D, Schauer A, Patel DK, Smith EF, Porter ME, Kner P, Lechtreck KF (2013). A differential cargo-loading model of ciliary length regulation by IFT. Curr Biol 23, 2463–2471.

Yanagisawa HA, Kamiya R (2004). A tektin homologue is decreased in *Chlamydomonas* mutants lacking an axonemal inner-arm dynein. Mol Biol Cell 15, 2105–2115.

Yang P *et al*. (2006). Radial spoke proteins of *Chlamydomonas* flagella. J Cell Sci 119, 1165–1174.